Cellular Oncology 31 (2009) 393–405
DOI 10.3233/CLO-2009-0484
IOS Press

Dual function microtubule- and mitochondria-associated proteins mediate mitotic cell death

Leyuan Liu, Rui Xie, Chaofeng Yang and Wallace L. McKeehan *

Center for Cancer and Stem Cell Biology, Institute of Biosciences and Technology, Texas A&M Health Science Center, Houston, TX, USA

Abstract. *Background*: Survival and evolution of aneuploid cells after an asymmetric segregation of chromosomes at mitosis may be the common initiating event and underlying cause of the genetic diversity and adaptability of cancers. We hypothesize that mechanisms exist to detect impending aneuploidy and prevent it before completion of an aberrant mitosis.

Methods: The distribution of isoforms of C19ORF5, an interactive partner with mitochondria-associated LRPPRC and tumor suppressor RASSF1A, state of spindle microtubules and mitochondrial aggregation was analyzed in synchronized mitotic cells and cells stalled in mitosis after treatment with paclitaxel.

Results: C19ORF5 distributed broadly across the mitotic spindle and reversibly accumulated during reversible mitotic arrest. Prolonged stabilization of microtubules caused an accumulation of a C19ORF5 product with dual MAP and MtAP properties that caused irreversible aggregation of mitochondria and death of mitotic cells.

Conclusion: Dual function microtubule-associated (MAP) and mitochondria-associated (MtAP) proteins generated by prolonged mitotic arrest trigger mitochondrial-induced mitotic cell death. This is a potential mechanism to prevent minimal survivable aneuploidy resulting from an aberrant cell division and cancers in general at their earliest common origin.

Keywords: Aneuploidy, C19ORF5, genetic instability, LRPPRC, microtubule dynamics, mitochondrial dynamics, RASSF1A, paclitaxel, tumor suppression, mitochondria aggregation

1. Introduction

Abnormal chromosome number (aneuploidy) resulting from an asymmetric chromosome segregation is the single genetic abnormality that is common to all tumor cells [1–4]. The symmetry of chromosome segregation at mitosis is dependent on mitotic spindle function and alignment of all chromosome pairs at the metaphase plate prior to onset of anaphase [5,6]. Capture and alignment of chromosomes by microtubules is a stochastic and asynchronous process. Elaborate short range, non-diffusible signals communicate the status of microtubule-chromosomal junctions to the anaphase-promoting complex/cyclosome (APC/C). The APC/C complex controls degradation of proteins that hinder chromosome separation and completion of mitosis. Mechanisms that monitor chromosome alignment are sufficiently sensitive to delay the onset of anaphase because of a single unaligned chromosome. Delays known as mitotic checkpoints are necessarily of limited duration so that already aligned chromosomes with bipolar attachments to relatively stable K-fiber spindle microtubule bundles hold in position at the plate while more dynamic microtubules continue to search for, capture and bring outliers into alignment [7]. If not for this relative stability of K-fiber microtubules, alignment of chromosomes would be an endless process. It is during the final stages of the alignment process that the threat of generation of a minimal non-lethal aneuploidy is the greatest should a cell division proceed.

Mitochondria transition between punctate foci and tubular structures through fusion and fission dynamics [8]. Few studies have addressed in detail the relationships between mammalian mitochondrial dynamics and mitochondrial spindle microtubule dynamics

*Corresponding author: Dr. Wallace L. McKeehan, Center for Cancer and Stem Cell Biology, Institute of Biosciences and Technology, Texas A&M Health Science Center, Houston, TX 77030-3303, USA. Tel.: +1 713 677 7510; Fax: +1 713 677 7512; E-mail: wmckeehan@ibt.tamhsc.edu.

during mitosis [9]. In previous reports, we described a novel complex of dual function MtAPs and MAP's involved in communication between the microtubular cytoskeleton and mitochondria during chromosome remodeling and mitosis [10]. Mitochondria-associated LRPPRC (LRP130) is an mtAP that affects mitochondrial gene expression and metabolism [11]. LRPPRC interacts directly or indirectly with three dual function MtAPs and MAPs. It interacts directly with dual function MAP and MtAP UXT [12,13] and C19ORF5 (also called MAP1S and RABP1) [10,14–16] and indirectly through C19ORF5 with the tumor suppressor RASSF1 [10,17]. When RASSF1 that normally resides on mitochondria appears on microtubules, its buildup causes microtubule stabilization and bundling similar to the drug paclitaxel [17]. C19ORF5 is distributed in the cytosol, but exists in multiple isoforms that conditionally appear on both microtubules and mitochondria [14]. At sufficient levels, one or more isoforms of C19ORF5 concentrate on mitochondria and cause progressive aggregation of mitochondria resulting in DNA degradation and cell death [14].

Isoforms of broadly expressed C19ORF5 that span 115 to 20 kDa in cells and tissues exhibit homology to and features of neuronal tissue-associated MAP1 proteins, MAP1A and MAP1B [14,18]. Similar to MAP1 proteins [19], C19ORF5 is expressed as the full length product deduced from cDNA and gives rise to diverse posttranslational products. In this study we examined the isoforms of C19ORF5 and their redistribution among cytosol, microtubules and mitochondria in interphase and mitosis. Our results suggest a mechanism for prevention of aneuploidy by mitochondria-induced death of mitotic cells prior to completion of an aberrant cell division. This is mediated by dual function MAPs and MtAPs that bridge spindle microtubule and mitochondrial dynamics.

2. Materials and methods

2.1. Immunoreagents

Antibodies for p-Histone H3 and β-actin were from Santa Cruz Biotechnology and Sigma Chemicals, respectively. Anti-C19ORF5 monoclonal antibody 4G1 was developed from purified GST-C19ORF5SC and recognized an epitope between C19ORF5 sequence D667 to S767 [14]. Anti-C19ORF5 polyclonal antibodies Magd and Mt were developed in rabbits with a synthetic peptide corresponding to the 25-residue C19ORF5 MAGD domain (F967-A991) and a purified C19ORF5 recombinant protein containing the microtubule association domain (MT) (Fig. 1A) [14]. The recombinant antigen was made from a construct of C19ORF5 sequence A867-E966 N-terminally tagged with GST that was expressed in *E. coli*, purified with GSH affinity chromatography, the GST was removed with thrombin and the released protein further purified by DNA affinity chromatography [14]. Specificity, titer and epitope for antibodies was tested by immunoblot screens of lysates and immunohistochemical analysis of cells transiently transfected with recombinant C19ORF5SC and products of shorter constructs tagged at the N-terminus with GFP [14]. The Magd and Mt antibodies were useful for immunoblotting and immunostaining, respectively.

2.2. C19ORF5 recombinant construct

All recombinant constructs used in transfection experiments contained GFP at the N-terminus. The construct coding for the counterpart of the C19ORF5 short chain (C19ORF5SC) band observed in cell extracts was approximated with the C-terminal 393 amino acid residues of C19ORF5 as described [14]. The GFP-tagged full length, GFP-C19ORF5FL, was constructed by replacement of the N-terminal sequence of the GFP-C19ORF5SC construct with an N-terminal 2.6-kb fragment from the full length cDNA of human C19ORF5 in the pSPORT1 vector (RZPD German Resource Center for Genome Research, Berlin, German). The GFP-C19ORF5SC DNA was linearized by a *Hin*dIII digestion at the downstream of the GFP tag, end-filled with Klenow fragment and then cut with *BstXI* which recognizes a site in the coding sequence for the C-terminal region of C19ORF5 to remove the N-terminus of C19ORF5SC. The 2.6-kb DNA sequence for the N-terminal portion of C19ORF5 was generated by *SalI* cut in the sequence immediately upstream of the translation initiation codon of full length C19ORF5 and then end-filled followed by re-digestion with *BstXI*. The 2.6-kb fragment was ligated into the linearized GFP-C19ORF5SC plasmid to form the GFP-C19ORF5FL through a blunt- and cohesive-end ligation. A GFP-labeled construct corresponding to the C19ORF5HC band in cell extracts coding for amino acid sequence M1-P799 was created directly by removal of the sequence between two *BamHI* sites in the GFP-C19ORF5FL plasmid fol-

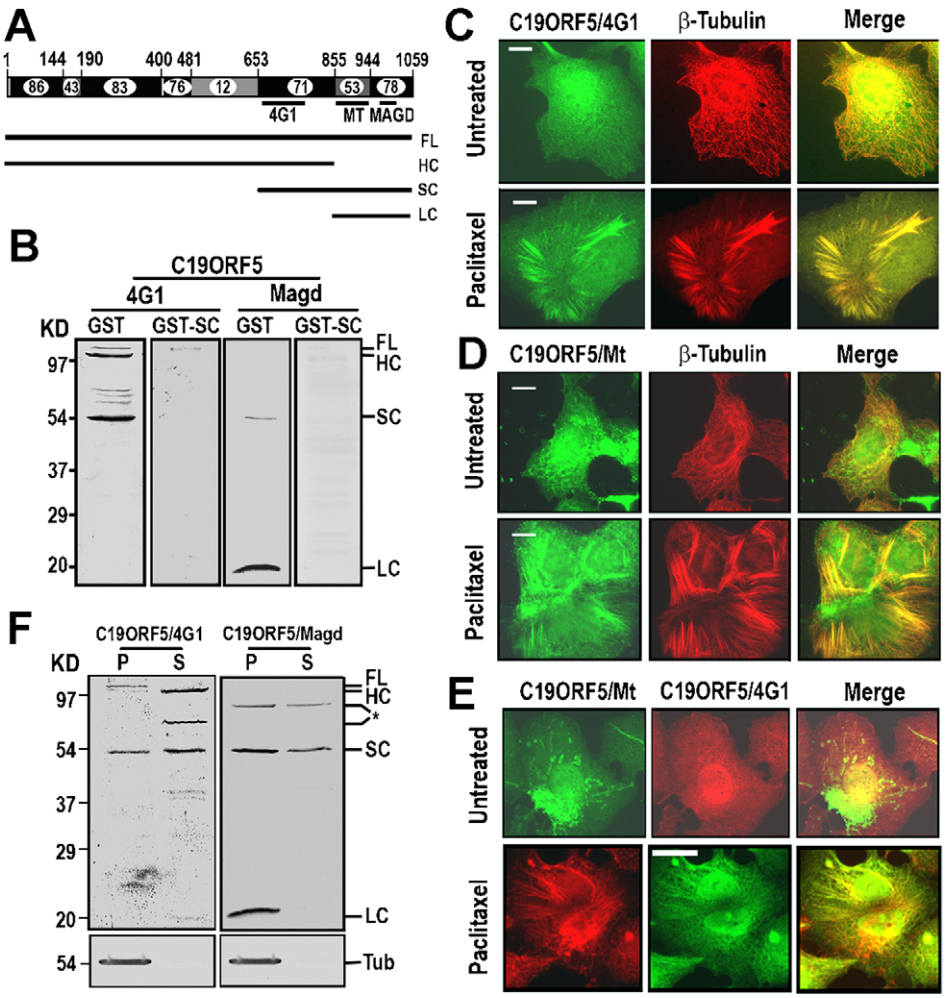

Fig. 1. Differential association of C19ORF5 isoforms with microtubules. (A) Human C19ORF5 isoforms estimated from immunoblots. Full length C19ORF5 was predicted from cDNA with amino acid sequence residues numbered from the initiation site. Percent identity of sequence between the indicated residues among *Homo sapiens*, *Macaca mulatta*, *Mus musculus* and *Rattus norvegicus* C19ORF5 is indicated. Epitope of the 4G1 monoclonal antibody has been mapped to the indicated region. The microtubule-association (MT) and MAGD domains against which Mt and Magd antibodies were directed [14] are also shown. FL, full length; HC, heavy chain; SC, short chain; and LC, light chain. (B) Profile of C19ORF5 isoforms in lysates of Hep3B cells revealed by 4G1 and Magd antibodies. Reaction mixtures were performed in the presence of 2 mg/ml purified GST or GST-C19ORF5SC (GST-SC) [14] as indicated. (C–E) Distribution of C19ORF5 in steady state and after paclitaxel-induced stabilization of microtubules. Hep3B cells were treated with 10 μM of paclitaxel for 12 h and stained with the 4G1, Mt and/or anti-β-tubulin antibody and visualized with FITC (green) or Rhodamine (red)-conjugated second antibody. Images were captured with an UltraPix cold CCD camera system through an Olympus IX70 inverted microscope using a 40×/1.35 oil objective. Yellow indicates intimate overlap of the two in the merge panels. Bar = 10 μm (all panels at the same magnification). (F) Differential association of C19ORF5 isoforms with microtubules *in vitro*. *In vitro* microtubule assembly and association of C19ORF5 isoforms from Hep3B cell lysates was performed by SDS-PAGE followed by immunoblot using the antibodies indicated in the text and visualized by secondary antibody conjugated with alkaline phosphatase as described [14,17]. P and S represent the respective pellet containing the microtubules and supernatant, respectively. Asterisks indicate unidentified C19ORF5 antigens. (The colors are visible in the online version of the article.)

lowed by re-ligation. The GFP-labeled recombinant correlate of the C19ORF5LC band in cell extracts coding for amino acids M842-F1059 was created by ligating the *Sma*I-digested pEGFP-C3 vector with an end-filled PCR product. The fidelity of constructs was confirmed by DNA sequence.

2.3. Cell transfection and siRNA

Except where indicated cells were grown on coverslips, processed, fixed and stained as previously described [14]. Monkey kidney COS7 cells were transiently transfected with GFP tagged C19ORF5 fusion

products constructed as described above by previously described methods [14]. HeLa cells were maintained in the same medium as COS7 cells but without kanamycin [10]. Double-stranded siRNA oligonucleotides were transfected into cells with Oligofectamine (Invitrogen) according to the manufacturer's recommended protocol.

2.4. Cell synchronization and fractionation

COS7 cells were cultured to 80% confluence in 75 cm^2 flasks containing 15 ml of culture medium as described [14], treated with 2 mM of a DNA replication inhibitor thymidine for 18 h to synchronize them in G1 [20], then released from the G1 block by removal of thymidine medium followed by one wash with fresh thymidine-free and then 8 h in fresh medium. The cells were arrested in mitosis by addition of 3.3 μM of the microtubule destabilizer, nocodazole, for 12 h. Unattached floating cells in the medium were removed by a gentle wash and the loosely attached mitotic cells were shaken off by tapping the flask vigorously 30 times after introduction of fresh medium. The remaining tightly attached interphase cells were scraped into lysis buffer [14] with a rubber policeman. About 2×10^5 shakeoff cells were seeded into a well with 2 ml of medium in new 6-well culture plates. Cells that reattached were scored as those capable of exiting mitosis. Test cultures were exposed to 3.33 μM nocodazole or the 26S proteasome inhibitor MG-132 as indicated. After five h, unattached and attached cells were again separated.

3. Results

3.1. C19ORF5 isoforms differentially associate with microtubules and mitochondria

C19ORF5 is widely expressed and appears in diverse forms that arise from a polyprotein precursor in lysates of cells and tissues (Fig. 1A) [14,15]. Monoclonal antibody 4G1 revealed antigens of apparent molecular masses between 115 and 55 KD in human hepatoma cells [14]. Lysates from human hepatoma Hep3B cells displayed the FL correlate at 115 KD, a strong 100 KD band and a 55 KD band as well as additional bands of less intensity between 100 and 55 KD (Fig. 1B). Polyclonal antibody (Magd) also revealed the 55 KD band and a 20 KD band (Fig. 1B). The competition of a recombinant GST-tagged correlate of the 55 KD band (SC in Fig. 1A) [14] in the immunoassays in contrast to GST alone and other unrelated C19ORF5 proteins indicated that the subject bands were all isoforms of C19ORF5. Subject bands were absent in cells derived from knockout mice devoid of C19ORF5 (unpublished results). We designated the 100 KD band the heavy chain (C19ORF5HC), the 55 KD band the short chain (C19ORF5SC) and the 20 KD band the light chain (C19ORF5LC) (Fig. 1A). Intermediate C19ORF5 antigens are being characterized.

Analysis of the cellular distribution of 4G1-reactive C19ORF5 isoforms that include the FL, HC and SC, but not the LC band in Hep3B cells indicated little association with steady-state interphase microtubules, but they concentrated on microtubules stabilized by paclitaxel (Fig. 1C). Polyclonal antibody Mt that recognized the recombinant FL, SC and LC forms, but not the HC isoform recapitulated the general distribution of endogenous C19ORF5 isoforms revealed by the 4G1 antibody (Fig. 1D). Quantitative aspects of the distribution were not identical (Fig. 1E) presumably because of differences in isoforms recognized by the two antibodies (Fig. 1A). An analysis with the 4G1 antibody of native isoforms from HepG2 cells [14] and Hep3B cells (Fig. 1F) indicated that both the FL and SC forms associated with paclitaxel-stabilized microtubules *in vitro* (Fig. 1F). The HC form was notably absent in the microtubule fraction. Analysis with the Magd antibody confirmed the association of the SC form with the microtubules and in addition revealed that the LC form also associated with the microtubule fraction (Fig. 1F). Together these results show that in addition to the full length polyprotein (FL) native C19ORF5 exists in HC, SC and LC isoforms in the human cell lines as well as other unidentified intermediates. The FL, SC and LC, but not the HC, associate with microtubules. The FL and SC forms do not associate extensively with microtubules in steady-state, but concentrate on stabilized microtubules.

We expressed and analyzed GFP-tagged recombinant correlates of the FL, HC, SC and LC forms estimated by size on SDS-PAGE and then observed distribution of the N-terminal GFP signal. The results with overexpressed N-terminally GFP tagged correlates of the identified C19ORF5 isoforms recapitulated and confirmed the isoform-dependent differences in interaction of native C19ORF5 isoforms with microtubules *in vitro* and in interphase cells (Fig. 2).

In separate experiments not shown here, we found that of the four recombinant isoforms, only C19ORF5SC caused mitochondria aggregation and cell death at elevated levels as previously described [14].

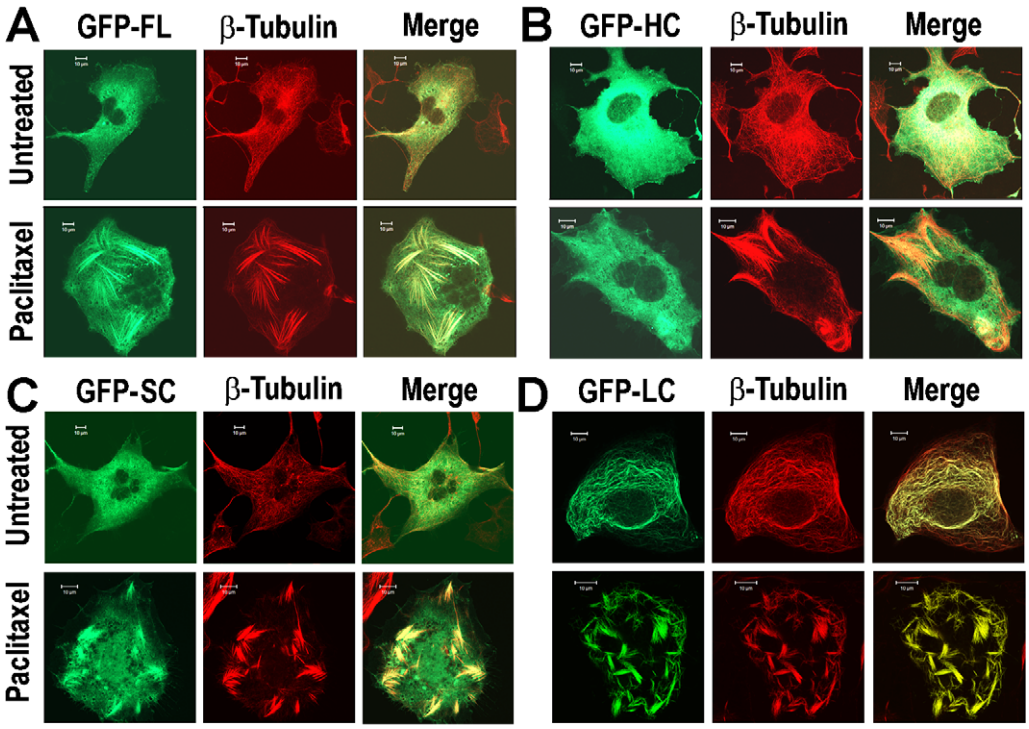

Fig. 2. Recombinant correlates recapitulate differential association of native C19ORF5 isoforms with microtubules. (A–D) GFP-tagged recombinant correlates of C19ORF5 full length (GFP-FL, A), heavy chain (GFP-HC, B), short chain (GFP-SC, C) and light chain (GFP-LC, D) estimated by the apparent molecular masses in Fig. 1A were constructed and transiently transfected into COS7 cells. Cells were treated overnight with 10 μM paclitaxel as indicated, microtubules visualized (red β-tubulin) and compared to the green GFP signal as in Fig. 1D, E. Images were captured with an inverted Zeiss LSM 510 laser scanning microscope equipped with a Plan-Apochromat 63×/1.4 oil immersion objective. Bar = 10 μm. (The colors are visible in the online version of the article.)

3.2. 4G1 and Mt-positive C19ORF5 isoforms distribute broadly across spindle microtubules and reversibly accumulate during mitotic arrest

The distribution and overlap with tubulin of C19ORF5 isoforms exhibiting the 4G1 and Mt epitopes was examined in cells in the four substages of mitosis. The 4G1 and Mt-positive C19ORF5 forms concentrated on the mitotic spindle and remained spread broadly across the entire apparatus throughout prophase to telophase. C19ORF5 remained associated with the spindle microtubules in cells arrested in mitosis with paclitaxel or the Eg5 kinesin inhibitor monastrol (Fig. 3A, B).

To examine C19ORF5 isoforms during mitosis, we synchronized cells and collected mitotic cells by shakeoff (Fig. 4A). In the absence of drug treatment, both interphase (Fig. 4B, S1) and mitotic cells (S2) exhibited similar levels of the four identified C19ORF5 isoforms (FL, HC, SC, LC). This indicated that the apparent increase in intensity of 4G1-positive C19ORF5 on the mitotic spindle in Fig. 3 reflected an accumulation of C19ORF5 on the spindle rather than an increase in total cellular C19ORF5.

Nocodazole blocks exit of mitosis by destabilizing microtubules and activates parameters associated with mitotic checkpoint delay [20]. Its application caused an increase in collective isoforms of C19ORF5 coincident with the increase in phosphorylated histone H3 (p-H3), a marker of cells in mitosis (Fig. 4B, S3, S4 vs. S1, S2). In the shakeoff fraction that was enriched in mitotic cells, the C19ORF5 FL, HC and SC forms increased 3 to 4-fold with no change in the LC form. Viable cells were captured by reattachment to culture substrate 5 h after washout of the nocodazole. About 22% of the nocodazole-treated shakeoff fraction reattached after removal of the nocodazole relative to about 6% of the shakeoff fraction that attached after 5 h of continued exposure to nocodazole (Fig. 4C). The reattached cells exhibited a reduction in all forms of C19ORF5 including the LC coincident with the decrease of p-H3 (Fig. 4B, S6 vs. S4). Noteworthy was a prominent unidentified 70 KD band (asterisk in Fig. 4B) that fluctuated among the

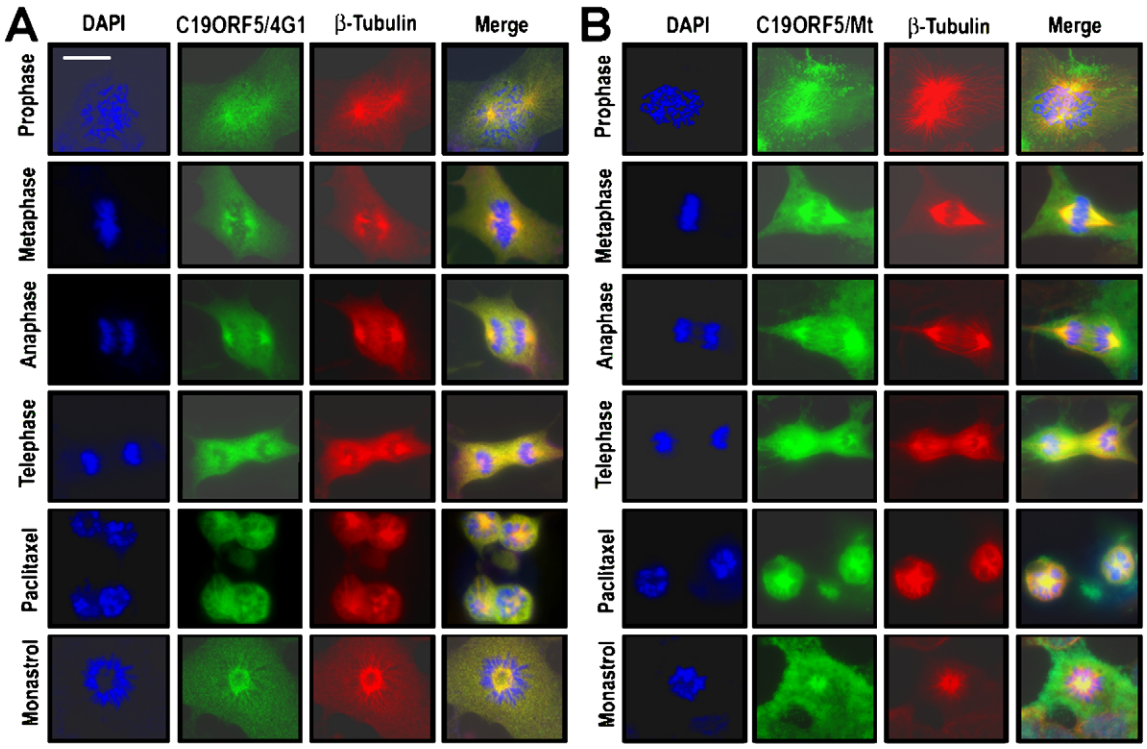

Fig. 3. Concentration and distribution of C19ORF5 across the mitotic spindle. (A, B) Cells at the indicated substages of mitosis were identified by morphology of chromosomes stained with DNA dye 4′,6-diamidino-2-phenylindole (DAPI). Degree of overlap (yellow) of 4G1- (A) or Mt-reactive C19ORF5 isoforms (B) revealed in green with β-tubulin-stained microtubules (red) was assessed in paclitaxel-arrested premetaphase cells or cells treated with monastrol as indicated. Images were captured using the cold CCD camera. Bar = 10 μm (panels at same magnification). (The colors are visible in the online version of the article.)

different conditions. Whether this and others are intermediates of processing to lower molecular weight isoforms or a degradative products remains to be established. When combined with the results in the last section, these results suggest that a large part of the existent and normally cytosolic C19ORF5 concentrates broadly along spindle microtubules during mitosis. Total C19ORF5 increases during mitotic arrest induced by the reversible microtubule destabilizer nocodazole. A significant number of cells exit mitosis and return to interphase concurrent with a return of interphase levels of C19ORF5 after removal of the nocodazole blockade.

Nocodazole activates a mitotic delay concurrent with inhibition of APC/C ubiquitin ligase activity that is essential for degradation of barriers to onset of anaphase and completion of mitosis by the 26S proteasome [21]. To determine whether levels of C19ORF5 were affected by the 26S proteasome, we examined the effect of the 26S proteasome inhibitor MG-132 [22] on the number of cells that exited mitosis and the levels of C19ORF5 isoforms after removal of the nocodazole block. Increasing concentrations of MG-132 increasingly blocked cells in the shakeoff fraction from exiting mitosis (Fig. 4C). Analysis of the fraction of cells that failed to attach to culture substrates confirmed they were blocked in mitosis and exhibited similar levels of FL, HC and SC (Fig. 4B, S8–S11 vs. S4). Again the increased levels of potential precursors or degradation products between the HC and SC bands were notable.

To determine whether C19ORF5 actively contributes to mitotic arrest or is a correlate of it, we suppressed expression levels to about 30% of normal in Hela cells with three different siRNA sequences (Fig. 4D). About 77% of Hela cells were in the shakeoff fraction from cells treated with 100 ng/ml nocodazole that is indicative of total cells capable of entry and exit from mitosis (Fig. 4E). The number of cells in mitosis was reduced to as low as 52% with one of the anti-C19ORF5 siRNA constructs. These results indicate that an accumulation in total C19ORF5, predominantly due to the FL, HC and SC isoforms, correlated with nocodazole-induced mitotic arrest. MG-132 prevented the degradation of these isoforms while causing

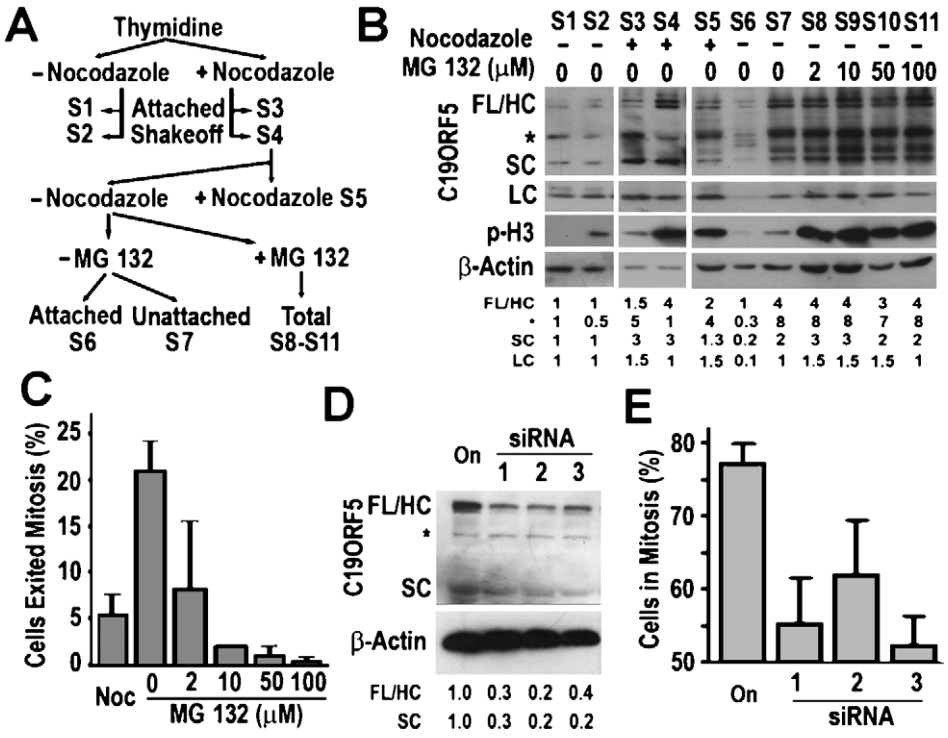

Fig. 4. Reversible accumulation of C19ORF5 during mitotic arrest. (A) Cell synchronization and sample preparation scheme. (B) Immunoblot of the samples prepared as in (A). An equal amount of protein from each sample determined with the Pierce BCA Protein Assay kit [14] was analyzed by immunoblot first with monoclonal antibody 4G1 (top panel) to assess FL, HC, SC and other unidentified products of C19ORF5 exhibiting the 4G1 epitope. Immunoblots were then stripped and stained with the Magd antibody to assess the LC isoform. A replicate membrane of the same samples prepared at the same time was stained with anti-p-Histone H3 (p-H3) antibody as a marker of mitosis. Immunoblots were stripped and analyzed with anti-β-actin as an additional control. Protein bands were visualized with the Amersham ECL Western Blotting Detection System. Relative amounts of C19ORF5 isoforms were estimated by densitometry using an AlphaImager system (Alpha Innotech) and expressed in units relative to untreated controls that were assigned a unit of one. (C) Inhibition of mitotic exit by the 26S proteasome inhibitor MG-32. Cells from the shakeoff fraction that exited mitosis were quantified by direct count of attached cells remaining after 5 h in new culture dishes. Results were expressed as a percent of attached cells divided by total cells seeded and represent the mean $\pm$ SD of three independent experiments. (D) C19ORF5 expression in HeLa cells was suppressed by Oligofectamine-assisted transfection with three different siRNAs targeting C19ORF5 mRNA (Silencer pre-designed siRNA-1, ID 26322; siRNA-2, ID 45347; and siRNA-3, ID 45439) and Silencer® Negative Control #1 siRNA purchased from Ambion. Cell lysates analyzed by immunoblot using the 4G1 antibody. The relative intensities of bands were estimated as described in (B). (E) Effect on number of cells in mitosis due to the siRNA treatments was estimated as a percent of mitotic cells subject to shakeoff divided by shakeoff and attached cells after 12 h exposure to 100 ng/ml nocodazole after cells were exposed to the siRNAs for 48 h. Results were expressed as a percent of shakeoff cells divided by the sum of shakeoff and attached cells and represent the mean $\pm$ SD three independent experiments.

the increase in intermediate bands between the molecular masses of HC and SC. The siRNA depression also suggests a potentially active role of one or more isoforms of C19ORF5 in mitotic progression.

3.3. *The C19ORF5SC isoform accumulates specifically during paclitaxel-induced mitotic arrest*

In contrast to nocodazole, mitotic arrest caused by the microtubule stabilizer RASSF1, an interaction partner of C19ORF5 [17], or paclitaxel is irreversible [5]. Both result in recruitment of the normally cytosolic C19ORF5 isoforms FL and SC to stabilized microtubules [14]. Therefore, we examined the effect of paclitaxel treatment on the cell cycle-dependent distribution of different C19ORF5 isoforms. In contrast to nocodazole treatment, exposure to 10 μM paclitaxel for 72 h after release of cultures from the G1 thymidine block resulted in up to 90 percent of the Hep3B, COS7 and Hela cell lines to appear in the combined shakeoff and unattached cell fractions (Fig. 5A, B). Inability of the pooled shakeoff and unattached cell population to attach and survive after introduction to fresh substrate

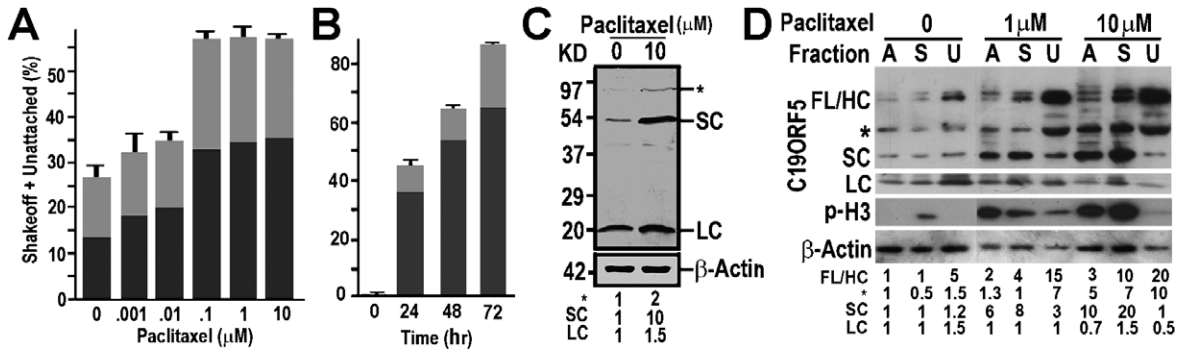

Fig. 5. Selective accumulation of C19ORF5SC after paclitaxel-induced mitotic arrest. (A, B) Irreversible mitotic arrest by paclitaxel. The indicated amounts of paclitaxel for 24 h (A) or 10 μM for the indicated times (B) was added to cells in fresh medium after release from the G1 thymidine block. Unattached (gray part of bars), shakeoff (solid part of bars) and remaining attached cells were counted and expressed as a percent of total. Results are from Hela cells that were representative of all cell types employed in this study. Results represent the mean ± SD of three independent experiments. (C) Immunoblot of Hep3B lysates with the anti-C19ORF5 Magd antibody after 24 h of exposure to paclitaxel. (D) Distribution of 4G1-reactive C19ORF5 isoforms during a paclitaxel block. Equal amounts of lysates based on protein content of attached (A), shakeoff (S) and unattached (U) COS7 cells were analyzed after treatment with paclitaxel at the indicated concentrations for 12 h subsequent to release from the thymidine block. The same membranes were reacted sequentially with anti-C19ORF5 4G1 and Magd antibodies and anti-p-Histone H3 (p-H3) to monitor mitotic cells. The relative amounts of C19ORF5 isoforms were estimated by densitometry as in Fig. 4A.

and culture medium confirmed the irreversibility of the treatment.

Analysis of C19ORF5 in lysates of HepG2 cells exposed to paclitaxel for 12 h with the Magd antibody revealed that the level of C19ORF5SC increased by 10 fold due to the paclitaxel treatment relative to the LC which increased by about 1.5 fold (Fig. 5C). This modest increase in LC was similar to that observed in the nocodazole block (Fig. 4B). Also worthy of note here is that the SC form that is about 10% of the LC form in interphase cells became equal to the relatively constant LC form after the paclitaxel treatment. A dose-dependent analysis of effect of paclitaxel on antibody 4G1- and Magd-reactive C19ORF5 isoforms in attached (A), shakeoff (S) and unattached (U) cell fractions confirmed a 20-fold accumulation of selectively the SC band in arrested cells (Fig. 5D). This was parallel to the lesser but expected increase in the FL and HC forms coincident with the increase in mitotic cells in both the attached and shakeoff fractions. The SC fraction along with p-H3 was markedly reduced in unattached paclitaxel-treated cells that are assumed to be in various stages of cell death and disintegration (Fig. 5D). These results suggest that the SC isoform selectively accumulates during a mitotic blockade caused specifically by prolonged stabilization of microtubules. This indicates that accumulation of SC is dependent on and proportional to degree of spindle microtubule stability.

3.4. Accumulation of C19ORF5SC during mitotic arrest is associated with irreversible aggregation of mitochondria

In cells in interphase when total C19ORF5 levels including the SC form are low and in steady-state (Figs 4, 5), mitochondria distribute in normal cytosolic reticular networks (Fig. 6A). In agreement with others [23], stabilization of microtubules by paclitaxel had no effect on the distribution or state of aggregation of the mitochondria in interphase cells (Fig. 6A). Similarly, mitochondrial distribution or aggregation was insensitive to the stabilization of microtubules by overexpression of the C19ORF5 partner, RASSF1A [17] or the recombinant correlate of the C19ORF5LC (results not shown). Furthermore, paclitaxel or RASSF1A had no apparent effect on mitochondrial dynamics in interphase cells expressing the recombinant C19ORF5SC correlate at low levels (Fig. 6C, D). C19ORF5-associated aggregation of mitochondria occurs only in cells proportional to levels of recombinant C19ORF5SC [14]. When the level of C19ORF5SC is elevated artificially it is capable of disruption of mitochondrial dynamics independent of dynamic state of microtubules. Thus hyperstabilization of microtubules appears to cause elevated levels of specifically C19ORF5SC that then causes mitochondrial aggregation. Under this condition the C19ORF5SC-associated tubular structures of mitochondria aligned

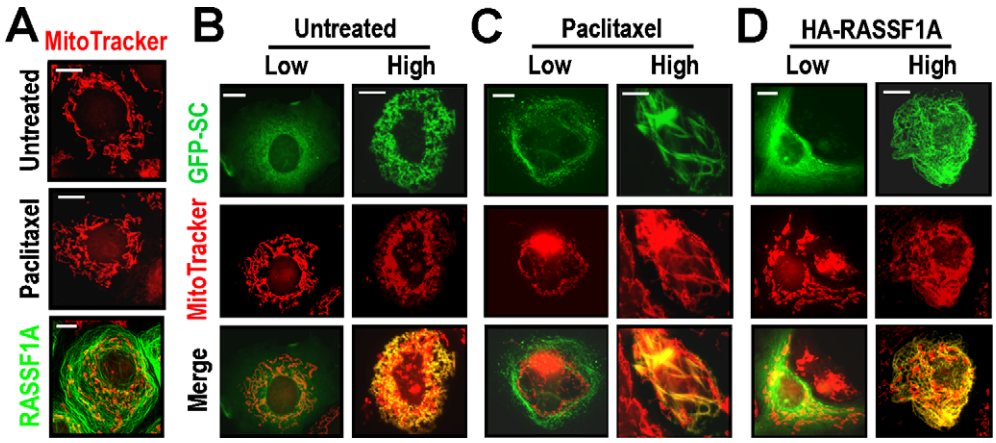

Fig. 6. C19ORF5-induced aggregation of mitochondria in Interphase cells. (A) Paclitaxel or RASSF1A alone does not disrupt mitochondrial distribution. COS7 cells were exposed to 10 μM paclitaxel overnight or transiently transfected with GFP-RASSF1A (green) for 48 h. Mitochondria were visualized with MitoTracker Red CMXRos (red). (B–D) C19ORF5SC causes mitochondrial aggregation independent of microtubule stabilization. Cells were transfected with GFP-SC untreated (B) or treated with 10 μM of paclitaxel (C) or co-transfected with RASSF1A tagged with HA at the N-terminus (D). Cells expressing low and high levels of C19ORF5SC based on intensity of the green GFP tag are shown. RASSF1A-positive cells were marked by the presence of hyperstabilized microtubules. Yellow indicates overlap of green GFP-SC with red MitoTracker-labeled mitochondria. Images were captured with the cold CCD camera. Bar = 10 μm (panels were at same magnification). (The colors are visible in the online version of the article.)

and overlapped with the fibrillar bundles of hyperstabilized microtubules (Fig. 6C, D).

We then examined the distribution and dynamics of mitochondria and 4G1- and Mt-reactive C19ORF5 during mitosis, mitotic arrest and mitotic cell death. During the four stages of a normal mitosis, mitochondria distributed around the spindle and the condensed chromosomes in normal reticular networks similar to those observed in interphase (Fig. 7A). Mitochondria were notably absent from areas of condensed chromatin but an overlap of mitochondria with spindle K-fiber bundles of microtubules was apparent in increasing intensity toward the centrosomes. A direct interaction at distinct sites between mitochondria and the spindle microtubules could not be determined because of limits in microscopic resolution.

Distribution of mitochondria was then analyzed in Hep3B cells after the paclitaxel treatment described in Fig. 5C which selectively elevated C19ORF5SC by 10 to 20 fold. Forty percent of attached cells were blocked in interphase and unable to enter mitosis (Fig. 6A). Twenty percent of cells that had a DNA content of 4N based on FACS analysis (data not shown) had apparently exited mitosis and exhibited distinct multi-nuclei and cytosol in which chromatin was no longer condensed (Fig. 7B, first panel, upper cell). Despite the gross nuclear and genomic derangement, mitochondria in these cells were dispersed into the normal reticular networks characteristic of interphase. The intensity of Mt-reactive C19ORF5 that exhibited overlap with mitochondria as well as dispersion in the cytosol was consistent with interphase levels of C19ORF5 in attached cells treated with paclitaxel (Fig. 5D). The third cell type that constituted about 40% of cells, was round in morphology, exhibited condensed chromosomes, and the Mt-reactive C19ORF5 and mitochondria reporter signals from it were most intense (Fig. 7B, boxed cell). An amplified view of these cells in the second panel at lower exposure revealed extensive C19ORF5-associated mitochondrial aggregates surrounding clearly condensed chromatin. No distinct nuclear membranes were apparent. These cells were clearly stuck in prometaphase. This indicates that the C19ORF5-associated mitochondrial aggregation only occurs in cells locked in mitotic arrest when the dual function MAP and MtAP C19ORF5SC isoform is highest. Cells in the shakeoff fraction from the paclitaxel-treated Hep3B cultures in which C19ORF5SC was elevated 20 times that of untreated cells (Fig. 5D) were characterized by the presence of extensive aggregates of mitochondria associated with 4G1-reactive C19ORF5 (Fig. 7C). In contrast unattached cells collected prior to harvest of the shakeoff cells that were in mitosis exhibited levels of C19ORF5SC near those of untreated cells (Fig. 7C, bottom panel). Distinct C19ORF5-associated mitochondrial aggregates were no longer apparent although elevated levels of 4G1-reactive C19ORF5 iso-

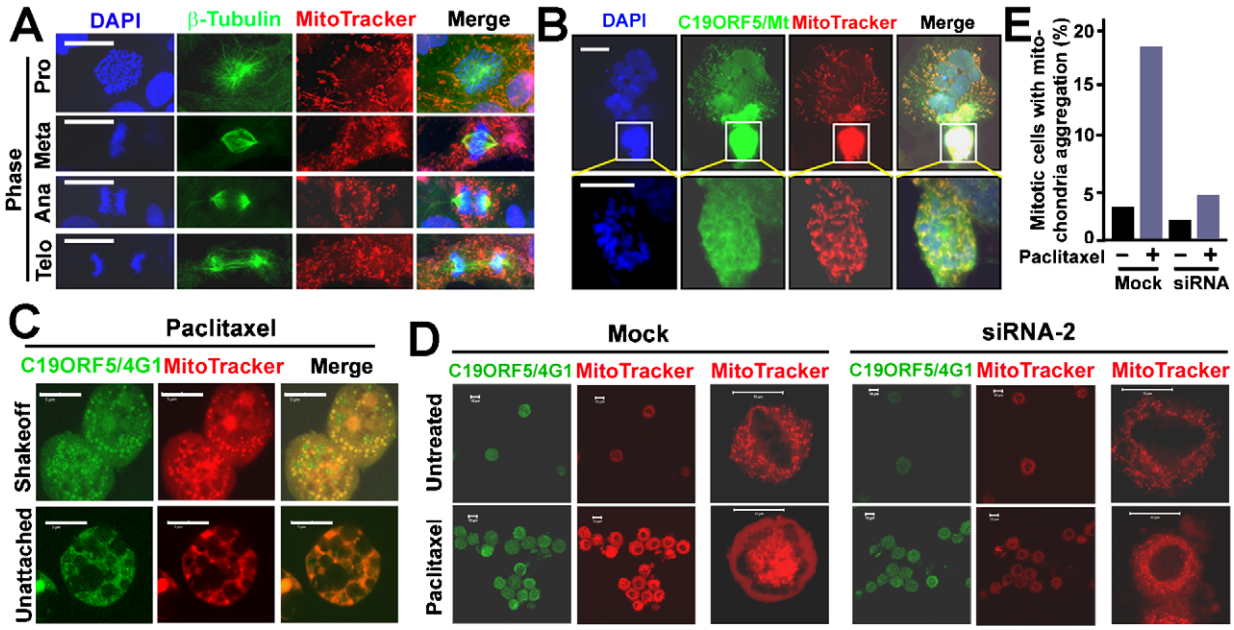

Fig. 7. C19ORF5-induced mitochondria aggregation during mitosis. (A) Normal mitochondrial distribution in relation to chromosomes and mitotic spindle. Hep3B cells in different substages of mitosis were identified by organization of DNA visualized with DAPI stain (blue). Spindle microtubules were visualized with anti-β-tubulin (green), and mitochondria in red with MitoTracker. (B) Distribution of C19ORF5 and mitochondria in paclitaxel-treated Hep3B cells. Hep3B cells were treated with 10 μM of paclitaxel overnight and attached cells were immunostained with DAPI to label DNA (blue), the Mt antibody to label C19ORF5 (green) and MitoTracker to label mitochondria (red). Cells blocked in interphase as shown in Fig. 6A, those blocked in premetaphase (boxed) and multinucleated cells that had apparently exited mitosis (upper cell) were scored based on state of their DNA revealed by DAPI stain (blue). The boxed cell is also shown in the second panel at reduced exposure. (C) Distribution of C19ORF5 protein and mitochondria in shakeoff and unattached paclitaxel-treated cells. Unattached and shakeoff Hep3B cells from cultures shown in Fig. 5D were collected by centrifugation at 300 rpm, resuspended in 1.5 ml tubes, fixed and stained at a stain to cell ratio similar to attached cells with antibody 4G1 to label C19ORF5 (green) and MitoTracker to label mitochondria (red) and plated on slides for observation. (D) Impact of C19ORF5 on mitochondria aggregation in mitotic cells. C19ORF5 expression in Hela cells were suppressed with siRNA #2 against C19ORF5 as described in Fig. 4D and treated with paclitaxel as in (B). C19ORF5 protein and mitochondria were traced with immunostaining with 4G1 antibody and MitoTracker, respectively. The images were captured at the same settings of exposure for 4G1 and MitoTracker for all four treatments so that the signal intensities for 4G1 and MitoTracker were comparable, respectively. The enlarged mitochondrial images were captured with optimized sets to visualize the mitochondria. (E) Percentage of mitotic cells with mitochondrial aggregation (as shown in the bottom panel of (D)) to total number of mitotic cells. Images in (A, B) were captured with the cold CCD camera while others were captured with the confocal. Bar = 10 μm (panels were at same magnification). (The colors are visible in the online version of the article.)

forms other than C19ORF5SC (Fig. 5D) were distributed across the cell. These cells likely represent late stages of mitotic death and disintegration due to prolonged mitotic arrest via microtubule stabilization.

3.5. *Suppression of C19ORF5 with siRNA abrogates paclitaxel-induced mitochondria aggregation and mitotic cell death*

To further test if the mitochondria aggregation in the paclitaxel-arrested premetaphase cells was caused by the associated C19ORF5SC accumulation, we used siRNA against C19ORF5 to suppress the C19ORF5 expression in Hela cells. The cells were treated with 10 μM paclitaxel for 12 h to block mitosis. Similar to Hep3B shakeoff cells, paclitaxel induced mitochondrial aggregation and intermingling with chromosomes, which was impeded when the C19ORF5 expression was suppressed with siRNA against C19ORF5 (Fig. 7D, E). Therefore, mitochondria aggregation in cells in which mitotic arrest was sufficiently prolonged was caused by the C19ORF5SC accumulation.

4. Discussion

Although the concept is nearly 100 years old [2], survival and evolution from a minimal aneuploidy resulting from a random or epigenetic-induced error in symmetric partition of chromosomes at mitosis is receiving renewed attention as the common initiating

event for all cancers [1,4]. Here we describe a potential cellular mechanism for prevention of aneuploidy mediated by a partnership between microtubule-associated proteins (MAP) and mitochondria-associated proteins (MtAP). Products of the C19ORF5 gene are part of a complex of interacting MAPs and MtAPs that include MtAPs LRPPRC and RASSF1 [10,17]. Isoforms of RASSF1 are conditional MAPs that appear on microtubules in association with one or more isoforms of C19ORF5 [17]. Concurrent appearance of RASSF1A and C19ORF5 on the mitotic spindle is associated with a delay in onset of anaphase [16]. The buildup of specifically RASSF1A that is suppressed by hypermethylation in a wide variety of tumors [24] has a paclitaxel-like stabilizing effect on microtubules that further results in accumulation of its interactive partner C19ORF5 on microtubules [17]. C19ORF5 confers specificity on the A isoform of RASSF1 for its microtubule interaction and stabilizing effects which suggests that the two act in a partnership [17].

We tested the hypothesis that one or more isoforms of C19ORF5 may exhibit dual function MAP and MtAP attributes that communicate stalled spindle microtubule dynamics to mitochondrial dynamics to induce mitochondria-dependent cell death in mitosis. The MAP or MtAP attributes of C19ORF5 are isoform-dependent. C19ORF5 FL and SC are conditional MAPs and associate with microtubules proportional to microtubule stability. The HC exhibited neither MAP nor MtAP properties. The LC associates with microtubules unconditionally and constitutively. Notably levels of the LC also remain constant relative to the other isoforms of C19ORF5. Neither of the FL, HC or LC isoforms exhibited an apparent association with mitochondria. Only the SC form conditionally exhibited dual MAP and MtAP properties.

We show that during mitosis C19ORF5 moved to the mitotic spindle apparatus from a predominantly cytosolic distribution [14]. This is in general agreement with others [16] except that our detection methods show that the distribution is relatively uniform during all phases of mitosis. The high intensity toward the centrosomes likely reflects the increased microtubule density at the poles. One or more isoforms of C19ORF5 may play a direct role in delay of the onset of anaphase [16]. Independent of whether C19ORF5 plays a direct regulatory role in mitotic progression or checkpoint delay, our data shows that collectively C19ORF5 reversibly accumulates during mitotic arrest. As cells exit mitosis, the return of all C19ORF5 isoforms back to interphase levels was sensitive to inhibition by the 26S proteasome.

We simulated prolonged mitotic arrest due to prolonged stabilization of spindle microtubules during a prolonged wait for the last chromosome to align with the irreversible microtubule stabilizing agent paclitaxel. Similar to nocodazole and other microtubule poisons that interfere with assembly of microtubules and chromosome attachment, paclitaxel triggers general parameters associated with mitotic checkpoint delay. However, paclitaxel specifically reveals the series of events resulting from the prolonged stabilization of spindle microtubules when the wait for complete chromosome alignment becomes unlimited. Paclitaxel also mimics the sustained stabilizing effect resulting from accumulation of MtAP RASSF1A on microtubules that appears to occur via a RASSF1A-C19ORF5 complex [16–18]. The elevation of collective isoforms of C19ORF5 due to the paclitaxel blockade further supported the idea that C19ORF5 generally accumulates in parallel with mitotic arrest. The 20-fold accumulation of specifically the dual function MAP and MtAP C19ORF5SC product that induces mitochondria aggregation and cell death [14] occurs only with the microtubule-stabilizing mode of mitotic arrest.

In mammalian cells, mitochondria movements during interphase and cell division are intimately interwoven with the dynamics of microtubules and therefore MAPs [9,25,26]. Similar to microtubules, mitochondria also exist in a dynamic state of elongation (fusion) and breakdown (fission) [8,23,27]. Mitochondria tubule homeostasis is maintained by the balance of fusion and fission forces mediated by MtAPs that act predominantly at intramitochondrial junctions. Both the large branching C19ORF5SC-induced aggregates of mitochondria in interphase and C19ORF5-associated aggregates resulting from the paclitaxel-induced mitotic blockade resemble the aggregated structures caused by overexpression of fusion promoter mitofusin (Mfn2) and the deficiency in fission-promoting dynamin-related protein (Drp1) [8]. Such structures represent subversion of the fission element of mitochondria dynamics sufficiently severe to cause irreversible hyperfusion of mitochondria tubules. Although accumulation of C19ORF5SC is dependent specifically on prolonged stabilization of spindle microtubules during prometaphase, C19ORF5SC-associated aggregation of mitochondria was notably independent on status of the microtubules if it was elevated independently. This is consistent with the independence of the mitochondria association and aggregation domain in C19ORF5 [14]. This suggested a direct action of C19ORF5SC on fission–fusion dy-

namics of mitochondria independent of direct association with microtubules. However, in the presence of paclitaxel or elevated levels of RASSF1A the C19ORF5-associated hyperfused tubules of mitochondria aligned with fibrillar bundles of stabilized microtubules. This may indicate a concurrent association of C19ORF5SC with mitochondria and microtubules despite the fact that mitochondria and microtubule association domains can be functionally dissected [14]. Whether C19ORF5-associated intermitochondrial and mitochondrial-microtubule junction points are overlapping together with factors as Mfn2 and Drp1 at mitochondrial tubule scission sites is under investigation.

In sum, we have described a mechanism whereby a survivable minimal aneuploidy can be prevented by induction of mitotic cell death before it happens as a result of completion of an aberrant cell division. This is mediated by cooperativity among dual function MAPs and MtAPs as RASSF1A and C19ORF5. A normally short-lived specific product of C19ORF5 accumulates due to prolonged stabilization of predominantly K-fiber bundles when cells are stuck in mitosis due to failure of alignment of the last chromosome. Accumulation of RASSF1A-C19ORF5 on the spindle past a certain threshold causes irreversible hyperstabilization of spindle microtubules. Resultant accumulation of C19ORF5SC causes hyper and irreversible fusion of mitochondria that causes mitotic cell death. Gross aneuploidy arising via an aberrant cell division is on average intrinsically lethal. However, our results suggest a natural mechanism that may limit the frequency of cancers at their earliest origin through prevention of a minimal survivable aneuploidy. This mechanism may also underlie the effectiveness of paclitaxel as a chemotherapeutic agent even in tumor cells that have become tolerant to high levels of aneuploidy.

Note added in proof

While this paper was in review, Liu et al., demonstrated that autophagy/mitophagy is robust during mitosis [28]. Histochemical marker analysis indicates the mitochondrial aggregates described in this study are largely cytochrome c-deficient mitochondria that accumulate due to blocked mitophagy.

Acknowledgements

We thank Dr. Le Sun and Joe Corvera (A&G Pharmaceuticals, Inc., Columbia, MD) for anti-C19ORF5 mouse monoclonal antibody 4G1. This work was supported by Public Health Service Grants CA59971 and DK35310 (WLM), DOD New Investigator Award W81XWH-08-1-0475 (LL), and aid from the John S. Dunn Research Foundation (WLM).

References

[1] P. Duesberg, Chromosomal chaos and cancer, *Sci. Am.* **296** (2007), 52–59.

[2] T. Boveri, *Zur Frage der Entstehung maligner Tumoren*, Gustav Fischer Verlag, Jena, Germany, 1914.

[3] P. Duesberg and D. Rasnick, Aneuploidy, the somatic mutation that makes cancer a species of its own, *Cell Motil. Cytoskel.* **47** (2000), 81–107.

[4] B.A. Weaver and D.W. Cleveland, Does aneuploidy cause cancer?, *Curr. Opin. Cell Biol.* **18** (2006), 658–667.

[5] P.K. Sorger, M. Dobles, R. Tournebize and A.A. Hyman, Coupling cell division and cell death to microtubule dynamics, *Curr. Opin. Cell Biol.* **9** (1997), 807–814.

[6] G.A. Pihan and S.J. Doxsey, The mitotic machinery as a source of genetic instability in cancer, *Semin. Cancer Biol.* **9** (1999), 289–302.

[7] S.L. Kline-Smith and C.E. Walczak, Mitotic spindle assembly and chromosome segregation: refocusing on microtubule dynamics, *Mol. Cell* **15** (2004), 317–327.

[8] A.E. Frazier, C. Kiu, D. Stojanovski, N.J. Hoogenraad and M.T. Ryan, Mitochondrial morphology and distribution in mammalian cells, *Biol. Chem.* **387** (2006), 1551–1558.

[9] M.P. Yaffe, N. Stuurman and R.D. Vale, Mitochondrial positioning in fission yeast is driven by association with dynamic microtubules and mitotic spindle poles, *Proc. Natl. Acad. Sci. USA* **100** (2003), 11424–11428.

[10] L. Liu, V. Amy, G. Liu and W.L. McKeehan, Novel complex integrating mitochondria and the microtubular cytoskeleton with chromosome remodeling and tumor suppressor RASSF1 deduced by in silico homology analysis, interaction cloning in yeast, and colocalization in cultured cells, *In Vitro Cell. Dev. Biol. Anim.* **38** (2002), 582–594.

[11] M.P. Cooper, L. Qu, L.M. Rohas, J. Lin, W. Yang, H. Erdjument-Bromage, P. Tempst and B.M. Spiegelman, Defects in energy homeostasis in Leigh syndrome French Canadian variant through PGC-1alpha/LRP130 complex, *Genes Dev.* **20** (2006), 2996–3009.

[12] H. Zhao, Q. Wang, H. Zhang, Q. Liu, X. Du, M. Richter and M.I. Greene, UXT is a novel centrosomal protein essential for cell viability, *Mol. Biol. Cell* **16** (2005), 5857–5865.

[13] T.N. Moss, A. Vo, W.L. McKeehan and L. Liu, UXT (Ubiquitously Expressed Transcript) causes mitochondrial aggregation, *In Vitro Cell. Dev. Biol. Anim.* **43** (2007), 139–146.

[14] L. Liu, A. Vo, G. Liu and W.L. McKeehan, Distinct structural domains within C19ORF5 support association with stabilized microtubules and mitochondrial aggregation and genome destruction, *Cancer Res.* **65** (2005), 4191–4201.

[15] Z. Orban-Nemeth, H. Simader, S. Badurek, A. Trancikova and F. Propst, Microtubule-associated protein 1S, a short and ubiq-

uitously expressed member of the microtubule-associated protein 1 family, *J. Biol. Chem.* **280** (2005), 2257–2265.

[16] M.S. Song, J.S. Chang, S.J. Song, T.H. Yang, H. Lee and D.S. Lim, The centrosomal protein RAS association domain family protein 1A (RASSF1A)-binding protein 1 regulates mitotic progression by recruiting RASSF1A to spindle poles, *J. Biol. Chem.* **280** (2005), 3920–3927.

[17] L. Liu, A. Vo and W.L. McKeehan, Specificity of the methylation-suppressed A isoform of candidate tumor suppressor RASSF1 for microtubule hyperstabilization is determined by cell death inducer C19ORF5, *Cancer Res.* **65** (2005), 1830–1838.

[18] A. Dallol, A. Agathanggelou, S.L. Fenton, J. Ahmed-Choudhury, L. Hesson, M.D. Vos, G.J. Clark, J. Downward, E.R. Maher and F. Latif, RASSF1A interacts with microtubule-associated proteins and modulates microtubule dynamics, *Cancer Res.* **64** (2004), 4112–4116.

[19] T.A. Schoenfeld, L. McKerracher, R. Obar and R.B. Vallee, MAP 1A and MAP 1B are structurally related microtubule associated proteins with distinct developmental patterns in the CNS, *J. Neurosci.* **9** (1989), 1712–1730.

[20] G. Fang, H. Yu and M.W. Kirschner, Direct binding of CDC20 protein family members activates the anaphase-promoting complex in mitosis and G1, *Mol. Cell* **2** (1998), 163–171.

[21] J.M. Peters, The anaphase promoting complex/cyclosome: a machine designed to destroy, *Nat. Rev. Mol. Cell Biol.* **7** (2006), 644–656.

[22] J. Zhao, T. Tenev, L.M. Martins, J. Downward and N.R. Lemoine, The ubiquitin-proteasome pathway regulates survivin degradation in a cell cycle-dependent manner, *J. Cell Sci.* **113**(23) (2000), 4363–4371.

[23] M. Muller, S.L. Mironov, M.V. Ivannikov, J. Schmidt and D.W. Richter, Mitochondrial organization and motility probed by two-photon microscopy in cultured mouse brainstem neurons, *Exp. Cell Res.* **303** (2005), 114–127.

[24] A. Agathanggelou, W.N. Cooper and F. Latif, Role of the Ras-association domain family 1 tumor suppressor gene in human cancers, *Cancer Res.* **65** (2005), 3497–3508.

[25] R.D. Vale, Intracellular transport using microtubule-based motors, *Annu. Rev. Cell Biol.* **3** (1987), 347–378.

[26] M.P. Yaffe, The machinery of mitochondrial inheritance and behavior, *Science* **283** (1999), 1493–1497.

[27] V.P. Skulachev, Mitochondrial filaments and clusters as intracellular power-transmitting cables, *Trends Biochem. Sci.* **26** (2001), 23–29.

[28] Liu et al., *Cell Cycle* **8**(10) (2009), in press.